AD-A150 217 GRID GENERATION FOR A PUMP COLLECTOR(U) PENNSYLVANIA STATE UNIV UNIVERSITY PARK APPLIED RESEARCH LAB G H HOFFMAN 04 OCT 84 ARL/PSU/TM-85-12 N00024-79-C-6043 1/1

UNCLASSIFIED F/G 20/4 NL

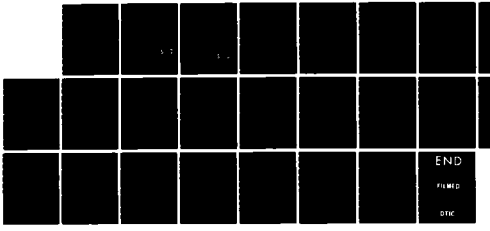

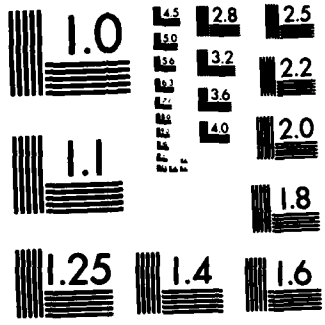

MICROCOPY RESOLUTION TEST CHART
NATIONAL BUREAU OF STANDARDS-1963-A

REPRODUCED AT GOVERNMENT EXPENSE

(6)

AD-A150 217

GRID GENERATION FOR A PUMP COLLECTOR

G. H. Hoffman

Technical Memorandum
File No. TM 85-12
4 October 1984
Contract N00024-79-C-6043

Copy No. 11

The Pennsylvania State University
Intercollege Research Programs and Facilities
APPLIED RESEARCH LABORATORY
Post Office Box 30
State College, Pa. 16804

DTIC ELECTE FEB 11 1985 S D B

DTIC FILE COPY

NAVY DEPARTMENT

NAVAL SEA SYSTEMS COMMAND

DISTRIBUTION STATEMENT A
Approved for public release;
Distribution Unlimited

85 01 30 016

GRID GENERATION FOR A PUMP COLLECTOR

G. H. Hoffman

Technical Memorandum
File No. TM 85-12
4 October 1984
Contract N00024-79-C-6043

Copy No. 11

The Pennsylvania State University
Intercollege Research Programs and Facilities
APPLIED RESEARCH LABORATORY
Post Office Box 30
State College, PA 16804

DTIC
ELECTE
FEB 11 1985
S D
B

Approved for Public Release

NAVY DEPARTMENT

NAVAL SEA SYSTEMS COMMAND

UNCLASSIFIED

SECURITY CLASSIFICATION OF THIS PAGE (When Data Entered)

REPORT DOCUMENTATION PAGE	READ INSTRUCTIONS BEFORE COMPLETING FORM
1. REPORT NUMBER: TM-85-12	2. GOVT ACCESSION NO.: AD-A150 217
	3. RECIPIENT'S CATALOG NUMBER
4. TITLE (and Subtitle): GRID GENERATION FOR A PUMP COLLECTOR	5. TYPE OF REPORT & PERIOD COVERED: Technical Memorandum
	6. PERFORMING ORG. REPORT NUMBER
7. AUTHOR(s): Gilbert H. Hoffman	8. CONTRACT OR GRANT NUMBER(s): N00024-79-C-6043
9. PERFORMING ORGANIZATION NAME AND ADDRESS: Applied Research Laboratory, P.O. Box 30, The Pennsylvania State University, State College, PA 16804	10. PROGRAM ELEMENT, PROJECT, TASK AREA & WORK UNIT NUMBERS
11. CONTROLLING OFFICE NAME AND ADDRESS: Naval Sea Systems Command, Code NSEA 63R31, Department of the Navy, Washington, DC 20362	12. REPORT DATE: 4 October 1984
	13. NUMBER OF PAGES: 32
14. MONITORING AGENCY NAME & ADDRESS(if different from Controlling Office)	15. SECURITY CLASS. (of this report): Unclassified
	15a. DECLASSIFICATION DOWNGRADING SCHEDULE

16. DISTRIBUTION STATEMENT (of this Report)

Approved for public release. Distribution unlimited.
Per NAVSEA - 25 October 1984.

17. DISTRIBUTION STATEMENT (of the abstract entered in Block 20, if different from Report)

18. SUPPLEMENTARY NOTES

19. KEY WORDS (Continue on reverse side if necessary and identify by block number)

grid generation
computational fluid dynamics
pumps

20. ABSTRACT (Continue on reverse side if necessary and identify by block number)

A simple scheme is presented which generates a surface-fitted grid for a pump collector with application to numerical solution of frozen vorticity flow inside the collector (the application to be covered in a later report). The scheme is two-dimensional in nature, but by a simplification of the collector geometry generates a three-dimensional grid. The procedure is very fast, requiring between two and three seconds of CPU time on an IBM 370/3033. Example grids are presented for several collector geometries.

DD FORM 1 JAN 73 1473 EDITION OF 1 NOV 65 IS OBSOLETE

UNCLASSIFIED

SECURITY CLASSIFICATION OF THIS PAGE (When Data Entered)

From: G. H. Hoffman

Subject: Grid Generation for a Pump Collector

Abstract: A simple scheme is presented which generates a surface-fitted grid for a pump collector with application to numerical solution of frozen vorticity flow inside the collector (the application to be covered in a later report). The scheme is two-dimensional in nature, but by a simplification of the collector geometry generates a three-dimensional grid. The procedure is very fast, requiring between two and three seconds of CPU time on an IBM 370/3033. Example grids are presented for several collector geometries.

DTIC COPY INSPECTED

Justification
By
Distribution/
Availability Codes
Dist | Avail and/or Special
A-1

I. Introduction

When solving any problem in fluid mechanics by finite difference methods, the first order of business is to generate a grid which fits the boundaries in the problem. A boundary fitted grid is essential to produce an accurate solution because the region in the vicinity of solid surfaces generally determines the character of the flow [1]*.

This report addresses the problem of generating a surface-fitted grid in a pump collector. This device, sketched in Figure 1, consists of an annular inlet ring connected to a doughnut-shaped chamber to which is attached a radial exit tube.

Because a pump collector is generally a three-dimensional geometry, the corresponding surface-fitted grid is also three-dimensional. To develop a capability for computing such a grid would require considerable time and effort. The development time can be reduced drastically by making two simplifying assumptions about the collector geometry. The resulting geometry will nevertheless be effective for conducting parametric studies of collector flows. The simplifying assumptions are as follows:

(1) The inlet ring and chamber as assumed to be axially symmetric. This means that the main portion of the device is formed by rotating the "inlet-chamber cross section" in the x-r plane about the θ axis.

(2) In the r-θ plane, the cross section of the exit tube is assumed to be rectangular instead of round. Also, the

*Numbers in brackets designate references [see p. 19]

profile in the x-r plane is assumed constant. Hence, the pipe is formed by rotating the x-r profile through an angle $\Delta\theta$.

Thus, a two-dimensional grid can be fitted to the cross sections of the simplified geometry and then rotated about the θ axis to produce a three-dimensional grid. ——→ 6 p 14 ?

Two basic approaches are available for generating two-dimensional surface-fitted grids. These are differential methods, represented by the work of Thompson and co-workers [2] and algebraic methods, represented by the work of Eiseman [3]. We shall extend the method of Amsden and Hirt [4] because of its simplicity and ease of application to the present problem. In the Amsden-Hirt procedure, the physical coordinates are taken to be solutions in the transformed plane of a linear elliptic system which consists of a modification of Laplace's equation with Dirichlet boundary conditions. This technique is well suited to our ultimate purpose -- to compute frozen vorticity flows in a collector -- because it generates a smoothly varying grid in the physical coordinates with a slowly varying mesh cell size.

II. Grid Generation Method

Inlet-Chamber Grid

The simplified inlet-chamber cross section is formed by a circle and a rectangle with one side of the rectangle tangent to the circle, as shown in Figure 2. A simple surface-fitted grid can be generated for this cross section by transforming the boundary into two connected rectangles. The original cross section is called the physical plane and the transformed rectangular cross section, the mapped plane. Inside the transformed cross section we overlay a network of rectangular grid lines of uniform spacing h,

which transforms to a system of curved grid lines in the physical plane. This process of generating the grid can be broken up into two steps:

(1) We prescribe the correspondence between points on the boundary in the mapped plane with those in the physical plane. This prescription is arbitrary and can be used to some extent to control distribution of grid lines in the physical plane.

(2) Next, we provide a prescription for determining the location of grid line intersections (vertices) in the physical plane which correspond to vertices in the mapped plane.

Thus, the process of grid generation proceeds backwards from the mapped plane with a rectangular boundary and grid to the physical plane with a curved boundary and grid. We will now cover the two steps of the process in detail.

The inlet-chamber cross section and grid can be conveniently described by the following parameters:

r_0 = radius of chamber circle in x-r plane

N_{LC} = number of grid intervals on chamber radius

N_A = number of intervals in width of inlet

N_{IN} = number of intervals in length of inlet

We start with a square in the mapped (ξ,η) plane with origin at the square center, as shown in Figure 3. Since the dimensions in the mapped plane are arbitrary, for convenience we choose the square to have a side of length two. Then the step size h in the mapped plane is

$$h = \frac{1}{N_{LC}} \quad . \tag{1}$$

and the collector inlet length ℓ and width w in the mapped plane are

$$\ell = h \cdot N_{IN} \quad , \tag{2}$$

$$w = h \cdot N_A \quad , \tag{3}$$

Using an (i,j) index system to designate (ξ,η) vertices, we have

$$\xi_i = -1 + (i-1)h \quad , \quad 1 \leq i \leq N_G + 1 \quad , \tag{4}$$

$$\eta_j = -1 + (j-1)h \quad , \quad 1 \leq j \leq N + 1 \quad , \tag{5}$$

where

$$N = 2N_{LC} \quad ,$$

$$N_G = N + N_{IN} \quad .$$

On the boundary in the mapped plane, corner points and critical control points are designated by the letters A-H (see Figure 3). Critical control points in this case are E and F which are, respectively, the point of tangency of the circle with the lower inlet segment and the point on the lower inlet segment directly beneath the junction of the circle with the upper inlet segment. We now must determine corresponding points A-H in the physical plane as well as all intermediate boundary vertices corresponding to intermediate boundary vertices in the mapped plane.

In the physical plane, we choose the origin of coordinates (x,r) at the center of the circle. The location of vertices on the bounding circle follows the simple prescription of Amsden and Hirt. As shown in Figure 4, we superimpose the square with side of length two on a circle with radius r_0 with common origin 0. Then, a straight line is passed through the origin and a

given boundary vertex on the square with coordinates $(\xi,\eta)_b$. The intersection of this line with the circle determines the corresponding boundary vertex $(x,r)_b$ in the physical plane.

The equation of the line is

$$\frac{r}{x} = \alpha \tag{6}$$

where

$$\alpha = \left(\frac{\eta}{\xi}\right)_b \equiv \text{given} \quad , \tag{7}$$

and the equation of the circle is

$$x^2 + r^2 = r_0^2 \quad . \tag{8}$$

The solution of these two equations gives $(x,r)_b$:

$$x_b = \pm \frac{r_0}{(1 + \alpha^2)^{1/2}} \quad , \tag{9}$$

$$r_b = \alpha\, x_b \quad , \tag{10}$$

where the sign of x_b is the same as the sign of ξ_b. If $\xi_b = 0$, then we have the special case

$$x_b = 0 \quad , \tag{11}$$

$$r_b = \pm\, r_0 \quad , \tag{12}$$

where the sign of r_b is the same as η_b. Thus, all of the vertices in the physical plane between A and E are determined from Eqs. (9) through (12).

Between boundary vertices E-F-G-H-A, associated with the inlet section, we space points uniformly. Thus, between E and F the boundary vertex coordinates are given by

$$x_b = \xi\left(\frac{x}{\xi}\right)_A = \xi\, x_A \quad , \quad 0 \leq \xi \leq 1 \quad , \tag{13}$$

$$r_b = - r_0 \quad . \tag{14}$$

Since vertex F is chosen to lie directly beneath vertex A in the physical plane, the lengths of sides FG and AH are the same. Hence, for uniform spacing the x coordinates of vertices on these boundary segments are the same. Thus,

$$x_b = x_F + r_0(\xi - \xi_F) = x_F + r_0(\xi - 1) \quad , \quad 1 \leq \xi \leq \xi_F \quad , \tag{15}$$

and

$$r_b = \begin{cases} - r_0 \text{ on FG} \\ r_A \text{ on AH} \end{cases} \quad . \tag{16}$$

On segment GH, the coordinates are

$$x_b = x_G \quad , \tag{17}$$

$$r_b = r_H + (\eta - \eta_H)\left(\frac{r_H - r_G}{\eta_H - \eta_G}\right) = r_H + (\eta - \eta_H)\left(\frac{r_H + r_0}{\eta_H + 1}\right) \quad , \quad \eta_A \geq \eta \geq -1 \quad . \tag{18}$$

With the inlet corner vertices F-G-H-A located in the physical plane, we can compute the inlet dimensions. The inlet length s, from Figure 2, is

$$s = x_G - x_F = r_0(\xi_G - 1) \quad , \tag{19}$$

and from Eqs. (1) and (4)

$$\xi_G = \frac{N_{IN} + N_{LC}}{N_{LC}} \quad . \tag{20}$$

Hence, the dimensionless inlet length in terms of the input parameters is

$$\frac{s}{r_0} = \frac{N_{IN}}{N_{LC}} \quad . \tag{21}$$

From Figure 2, the inlet width t is seen to be

$$t = r_0 + r_A \quad , \tag{22}$$

where r_A is obtained from Eq. (10) evaluated at boundary vertex A, viz.

$$r_A = \alpha_A x_A = \frac{\alpha_A r_0}{(1 + \alpha_A^2)^{1/2}} \quad . \tag{23}$$

From Eqs. (5) and (7), we find that α_A is

$$\alpha_A = \eta_A = -1 + \frac{N_A}{N_{LC}} \quad . \tag{24}$$

Then, combining Eqs. (23) and (24), the dimensionless inlet width is

$$\frac{t}{r_0} = 1 - \frac{1 - \frac{N_A}{N_{LC}}}{\left[1 + \left(1 - \frac{N_A}{N_{LC}}\right)^2\right]^{1/2}} \quad . \tag{25}$$

Solving Eq. (25) for N_A/N_{LC}, we obtain

$$\frac{N_A}{N_{LC}} = 1 - \frac{t/r_0}{\left[1 - \left(1 - t/r_0\right)^2\right]^{1/2}} \quad . \tag{26}$$

The inlet-chamber geometry dictates that N_A and N_{LC} both must be positive, i.e., $N_A/N_{LC} > 0$. When this ratio is zero, we find that

$$\frac{t}{r_0} = 1 - \frac{1}{\sqrt{2}} = 0.2928932$$

which is the minimum admissible value of t/r_0 for this mapping scheme. This lower limit is a consequence of how the vertices on the square are mapped to vertices on the circle and corresponds to the situation when line OP in Figure 4 intersects the lower right-hand corner of the square. This limit can be removed by using a different scheme to locate the vertices on the circle.

In the determination of the location of interior vertices, our main interest is to provide a prescription that will give a smooth variation of vertex locations and, consequently, a smooth variation of the metric coefficients. For the present application to the calculation of inviscid flow fields where flow gradients are not large, the simplest such prescription will be suitable.

Amsden and Hirt chose a simple prescription for locating an interior vertex as the average position of its eight nearest neighbors. A still simpler formula, which Amsden and Hirt showed gives nearly identical results to the "eight formula," is to place the interior vertex at the average location of its north-south and east-west neighbors. Thus, if we define a two-component column vector $z_{i,j}$ by

$$z_{i,j}^T = [x,r]_{i,j} \quad , \tag{27}$$

then the vertex coordinates by the latter formula are given by

$$z_{i,j} = \frac{1}{4}\left(z_{i-1,j} + z_{i,j-1} + z_{i+1,j} + z_{i,j+1}\right) \quad . \tag{28}$$

Equation (28) is the so-called unit square formula and is the finite difference solution using central difference approximations of

$$\frac{\partial^2 z}{\partial \xi^2} + \frac{\partial^2 z}{\partial \eta^2} = 0$$

on a uniform grid in ξ and η.

In the location of interior vertices, we will use the unit square formula. Amsden and Hirt solved for the $z_{i,j}$ by point relaxation, but a more efficient method is to put Eq. (28) into tridiagonal form so that single line overrelaxation (SLOR) may be used. Thus, along i = constant lines, we have

$$z_{i,j-1} - 4z_{i,j} + z_{i,j+1} = R_{i,j} \quad , \tag{29}$$

where R_j is a two-component column vector of known quantities given by

$$R_{i,j} = - z_{i-1,j} - z_{i+1,j} \quad . \tag{30}$$

In the relaxation sweep, for the direction of i increasing, the latest known values of z are used to evaluated $R_{i,j}$.

Along line i specification of the boundary conditions at j = 1 and $j = j_{max}$ (boundary vertices) closes the tridiagonal system. A solution of this linear system of equations is then obtained by the usual L-U decomposition procedure [5].

By performing numerical experiments, the optimum relaxation factor for the collector grid was found to be 1.5. This value was used in all ensuing calculations. Two examples are presented here for grids with step sizes suitable for inviscid calculations. Table I lists the parameters for these examples.

Case	r_0	N_{LC}	N_{IN}	N_A	s/r_0	t/r_0
1	1.0	10	10	4	1.0	0.4855
2	1.0	10	10	10	1.0	1.0

Table I. Collector Grid Geometry Parameters.

In both examples the number of iterations required for convergence was 28 and the CPU time on the PSU IBM 370/3033 was 2.3 seconds. Convergence was considered achieved when the maximum change in $x_{i,j}$ and $r_{i,j}$ during succeeding relaxation sweeps was less than 10^{-4}. Case 1 is shown in Figure 5 and Case 2 in Figure 6.

Exit Pipe Grid

The exit pipe profile in the x-r plane is assumed to be symmetric about x = 0 and is made up of three straight-line segments plus a circular arc, as shown in Figure 7. The exit pipe boundary A'-B'-C'-D' is transformed into a rectangle over which is laid a uniform rectangular mesh. The steps for generating this grid are similar to those for generating the inlet-chamber grid.

To describe the exit pipe profile and grid, the following parameters are required in addition to r_0 and N_{LC}:

N_{OW} = number of intervals in half width of exit pipe profile

N_{OL} = number of intervals in length of exit pipe

β = ratio of exit pipe final width W_2 to initial width W_1 [see Figure 7].

A restriction on the geometry of the exit pipe profile is that points A' and D' must lie between points B and C on the chamber arc. The reason for this is that B and C transform into the corners of a square in the mapped plane and, hence, A' and D' cannot lie outside these points. This restriction means that

$$N_{OW} \leq N_{LC} \quad .$$

The half width W_1 of the exit pipe profile at the chamber arc intersection is given by

$$W_1 = x_{A'} = \frac{r_0}{(1 + \alpha_{A'}^2)^{1/2}} \quad , \tag{31}$$

where

$$\alpha_{A'} = \frac{1}{\xi_{A'}} = \frac{1}{N_{OW}h} = \frac{N_{LC}}{N_{OW}} \quad . \tag{32}$$

and the half width W_2 of the profile at B'C' (flow exit) is

$$W_2 = \beta W_1 \quad . \tag{33}$$

We now proceed to assign vertices on the boundary in the physical plane corresponding to those in the mapped plane. On the circular arc A'-D', the vertices coincide with those on the chamber circle between A' and D'. The coordinates of these vertices are given by Eqs. (9)-(12). On A'-B' and C'-D', the sides of the exit pipe profile, we prescribe a uniform distribution of vertices in the physical plane according to

$$x = \pm \left[x_{A'} - \left(\frac{x_{A'} - x_{B'}}{\eta_{B'} - 1}\right)(\eta - 1)\right] \quad , \tag{34}$$

$$r = r_{A'} - \left(\frac{r_{A'} - r_{B'}}{\eta_{B'} - 1}\right)(\eta - 1) \quad , \tag{35}$$

where

$$x_{B'} = W_2 \quad , \tag{36}$$

$$r_{B'} = r_0 \eta_{B'} \quad , \tag{37}$$

$$\eta_{B'} = N_{OL}h = \frac{N_{OL}}{N_{LC}} \quad . \tag{38}$$

On B'-C', the end of the exit pipe, we also prescribe a uniform distribution of vertices, viz.,

$$x = \left(\frac{x_{B'}}{\xi_{B'}}\right) \xi \quad , \tag{39}$$

$$r = r_{B'} \quad . \tag{40}$$

The interior vertices are located using the unit square formula, Eq. (28), and the resulting tridiagonal system of equations is solved by SLOR with sweeps in the ξ direction.

Two examples of exit pipe profile grids are presented for the geometric and grid parameters given in Table II.

Case	r_0	N_{LC}	N_{OL}	N_{OW}	β
1	1.0	10	10	10	1.0
2	1.0	10	10	10	0.5

Table II. Exit Pipe Profile Grid Geometry Parameters.

In both cases, the number of iterations required for convergence, using the same criterion as for the collector, was 17 and the CPU time was 0.9 seconds. Case 1 is shown in Figure 8 and Case 2 in Figure 9.

III. Application to Calculation of a Flow Field

In this section we shall discuss in general terms how the previous grid generation scheme can be used in the numerical calculation of a collector flow field. We start with the strong conservation law form of the equations of fluid mechanics, which in cylindrical polar coordinates can be written as

$$\frac{\partial E}{\partial x} + \frac{\partial F}{\partial r} + \frac{\partial G}{\partial \theta} = H \quad , \tag{41}$$

where E, F, G, and H are vectors made up of the various conserved flow quantities. New independent variables ξ and η, which produce a grid fitted to the inlet-chamber cross section and exit pipe profile in the x-r plane, are introduced by the transformation

$$\xi = \xi(x,r) \quad , \quad \eta = \eta(x,r) \quad . \tag{42}$$

We want to show that Eq. (41) can be transformed into a strong conservation form in the (ξ,η,θ) coordinate system, which can then be used as the basis for numerical calculations.

The derivatives with respect to (x,r,θ) are related to those with respect to (ξ,η,θ) by the chain rule relations:

$$\frac{\partial}{\partial x} = \xi_x \frac{\partial}{\partial \xi} + \eta_x \frac{\partial}{\partial \eta} \quad , \tag{43}$$

$$\frac{\partial}{\partial r} = \xi_r \frac{\partial}{\partial \xi} + \eta_r \frac{\partial}{\partial \eta} \quad , \tag{44}$$

where subscripts denote partial differentiation with respect to the particular variable. Upon application of the chain rule relations, Eq. (41) becomes, after rearrangement

$$\left(\xi_x \frac{\partial E}{\partial \xi} + \xi_r \frac{\partial F}{\partial \xi}\right) + \left(\eta_x \frac{\partial E}{\partial \eta} + \eta_r \frac{\partial F}{\partial \eta}\right) + \frac{\partial G}{\partial \theta} = H \quad . \tag{45}$$

For later convenience, let us replace ξ_x, ξ_r, etc. to x_ξ, x_η, etc. by use of the chain rule. If we operate on x in Eqs. (43) and (44), a pair of linear equations for x_ξ and x_η results for which the solution is

$$Jx_{\xi} = \eta_r \quad , \tag{46}$$

$$Jx_{\eta} = -\xi_r \quad , \tag{47}$$

where J is the Jacobian of the transformation defined by the following determinant:

$$J = \begin{vmatrix} \xi_x & \eta_x \\ \xi_r & \eta_r \end{vmatrix} = \xi_x \eta_r - \xi_r \eta_x \quad . \tag{48}$$

Similarly, by operating on r in Eqs. (43) and (44), we get a pair of linear equations for r_{ξ} and r_{η} which has the following solution:

$$Jr_{\xi} = -\eta_x \quad , \tag{49}$$

$$Jr_{\eta} = \xi_x \quad . \tag{50}$$

Equations (46) through (50) are used to replace ξ_x, etc. by x_{ξ}, etc. in Eq. (45). Thus, Eq. (45) becomes

$$J\left(r_{\eta} \frac{\partial}{\partial \xi} - x_{\eta} \frac{\partial F}{\partial \xi}\right) + J\left(- r_{\xi} \frac{\partial E}{\partial \eta} + x_{\xi} \frac{\partial F}{\partial \eta}\right) + \frac{\partial G}{\partial \theta} = H \quad . \tag{51}$$

To simplify Eq. (51), the following identities are needed:

$$\left.\begin{aligned} r_{\eta} \frac{\partial E}{\partial \xi} &= \frac{\partial}{\partial \xi}\left(r_{\eta} E\right) - E r_{\xi\eta} \\ - x_{\eta} \frac{\partial F}{\partial \xi} &= - \frac{\partial}{\partial \xi}\left(x_{\eta} F\right) + F x_{\xi\eta} \\ - r_{\xi} \frac{\partial E}{\partial \eta} &= - \frac{\partial}{\partial \eta}\left(r_{\xi} E\right) + E r_{\xi\eta} \\ x_{\xi} \frac{\partial F}{\partial \eta} &= \frac{\partial}{\partial \eta}\left(x_{\xi} F\right) - F x_{\xi\eta} \end{aligned}\right\} \quad . \tag{52}$$

Then, Eq. (51) becomes

$$J \frac{\partial}{\partial \xi} \left(r_\eta E - x_\eta F \right) + J \frac{\partial}{\partial \eta} \left(- r_\xi E + x_\xi F \right) + \frac{\partial G}{\partial \theta} = H \quad . \tag{53}$$

The final transformed strong conservation form is obtained from Eq. (53) by dividing through by J, noting that $J = J(\xi, \eta)$ and defining the following transformed vectors:

$$\hat{E} = r_\eta E - x_\eta F \quad , \tag{54}$$

$$\hat{F} = - r_\xi E + x_\xi F \quad , \tag{55}$$

$$\hat{G} = G J^{-1} \quad , \tag{56}$$

$$\hat{H} = H J^{-1} \quad . \tag{57}$$

Then, the result is

$$\frac{\partial \hat{E}}{\partial \xi} + \frac{\partial \hat{F}}{\partial \eta} + \frac{\partial \hat{G}}{\partial \theta} = H \quad . \tag{58}$$

Equation (58) thus holds in a coordinate system for which the solid boundaries are families of the coordinates. Also, from Eq. (58) an appropriate finite difference algorithm can be derived which will be described in a later report.

In the numerical solution of Eq. (58), the metric coefficients x_ξ, x_η, r_ξ and r_η are required in Eqs. (54) through (57). Since the step size in the ξ-η plane is a constant, simple central difference expressions of second-order accuracy can be used to compute these quantities, viz.

$$(z_\xi)_{i,j} = \frac{z_{i+1,j} - z_{i-1,j}}{2h} + O(h^2) \quad , \tag{59}$$

$$(z_\eta)_{i,j} = \frac{z_{i,j+j} - z_{i,j-1}}{2h} + O(h^2) \quad , \tag{60}$$

where z is defined by Eq. (27). These derivatives need to be computed only once for a given geometry and then stored for later use in the fluid mechanical calculation.

REFERENCES

1. Thames, F. C., J. F. Thompson, C. W. Mastin and R. L. Walker, "Numerical Solutions for Viscous and Potential Flow about Arbitrary Two-Dimensional Bodies using Body-Fitted Coordinate Systems," Jour. Comp. Phys. 24:245 (1977).

2. Thompson, J. F., F. C. Thames and C. W. Mastin, "Boundary-Fitted Curvilinear Coordinate Systems for Solution of Partial Differential Equations on Fields Containing any Number of Arbitrary Two-Dimensional Bodies," NASA CR-2729 (July 1977).

3. Eiseman, P. R., "Geometric Methods in Computational Fluid Dynamics," Institute for Computer Applications in Science and Engineering Report No. 80-11 (April 1980).

4. Amsden, A. A. and C. W. Hirt, "A Simple Scheme for Generating General Curvilinear Grids," Jour. Comp. Phys. 11:348 (1973).

5. Keller, H. B., "Accurate Difference Methods for Nonlinear Two-Point Boundary Value Problems," SIAM Jour. Numer. Anal. 11:305 (1974).

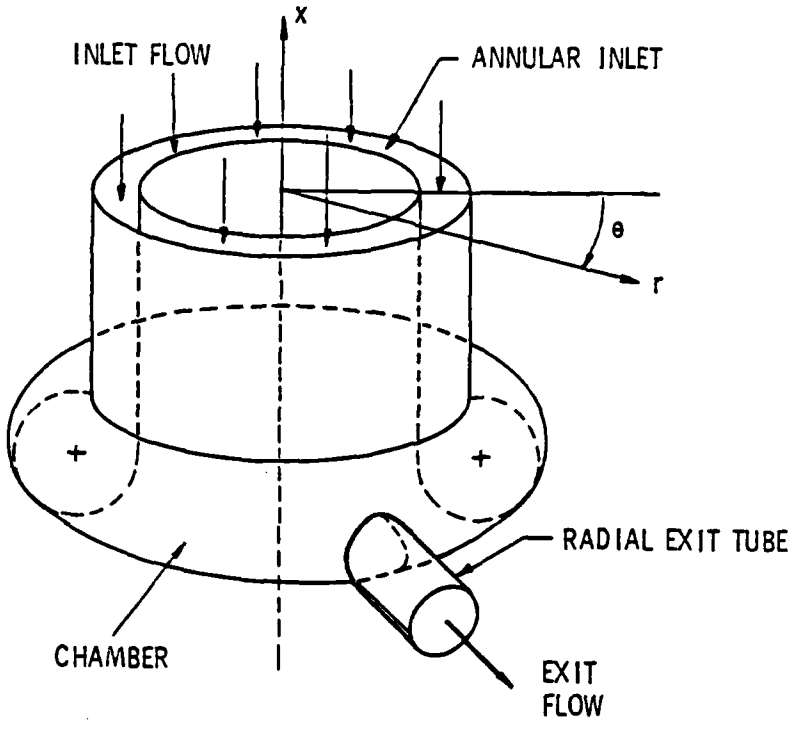

Fig. 1. Geometry for a Pump Collector.

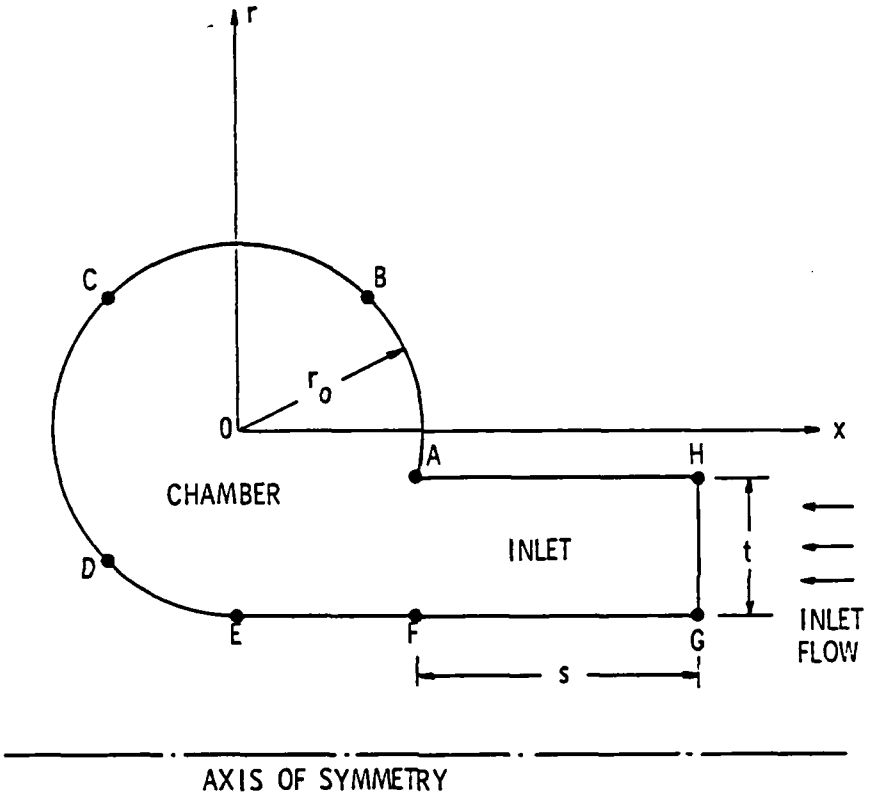

Fig. 2. Geometry of Simplified Inlet-Chamber Cross Section.

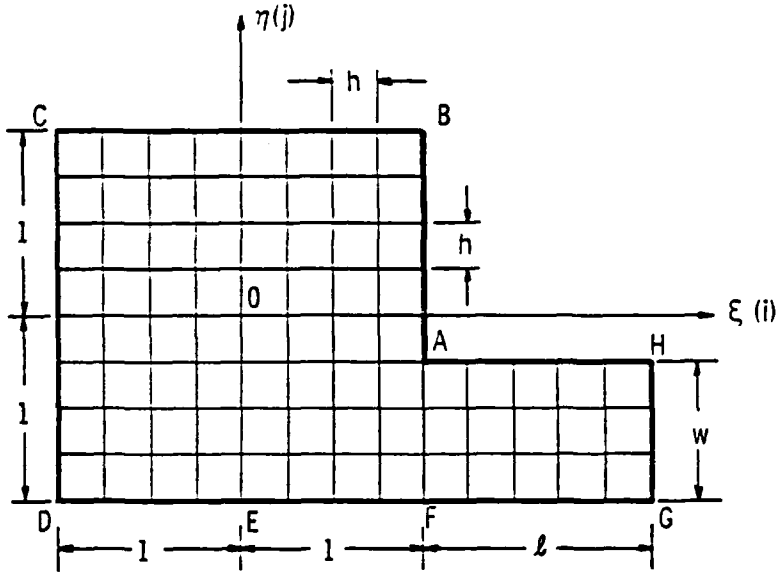

Fig. 3. Transformed Inlet-Chamber Cross Section Geometry and Grid.

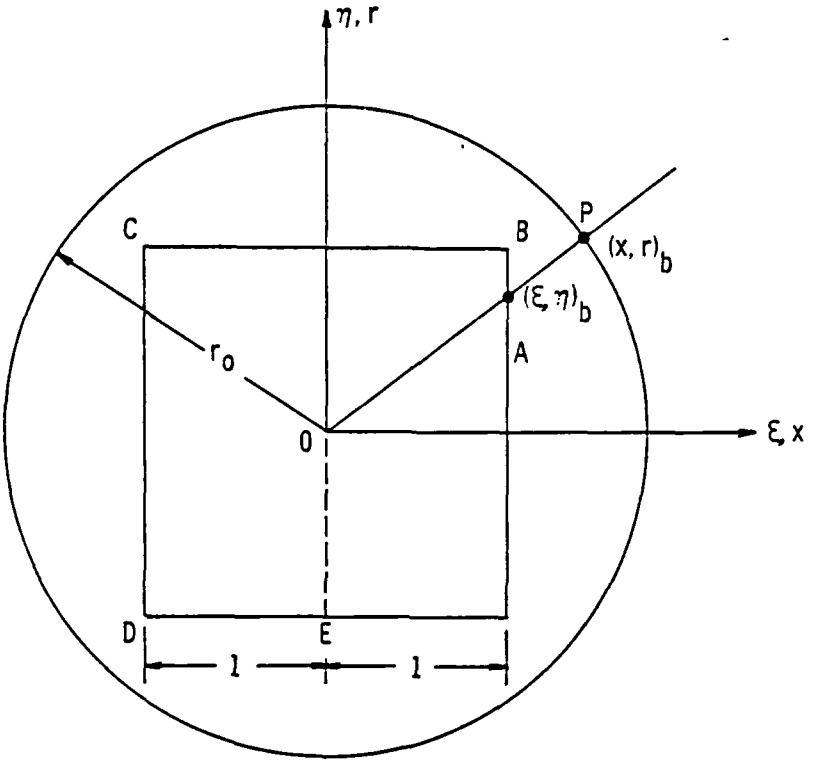

Fig. 4. Method of Locating Vertices on Circle Boundary.

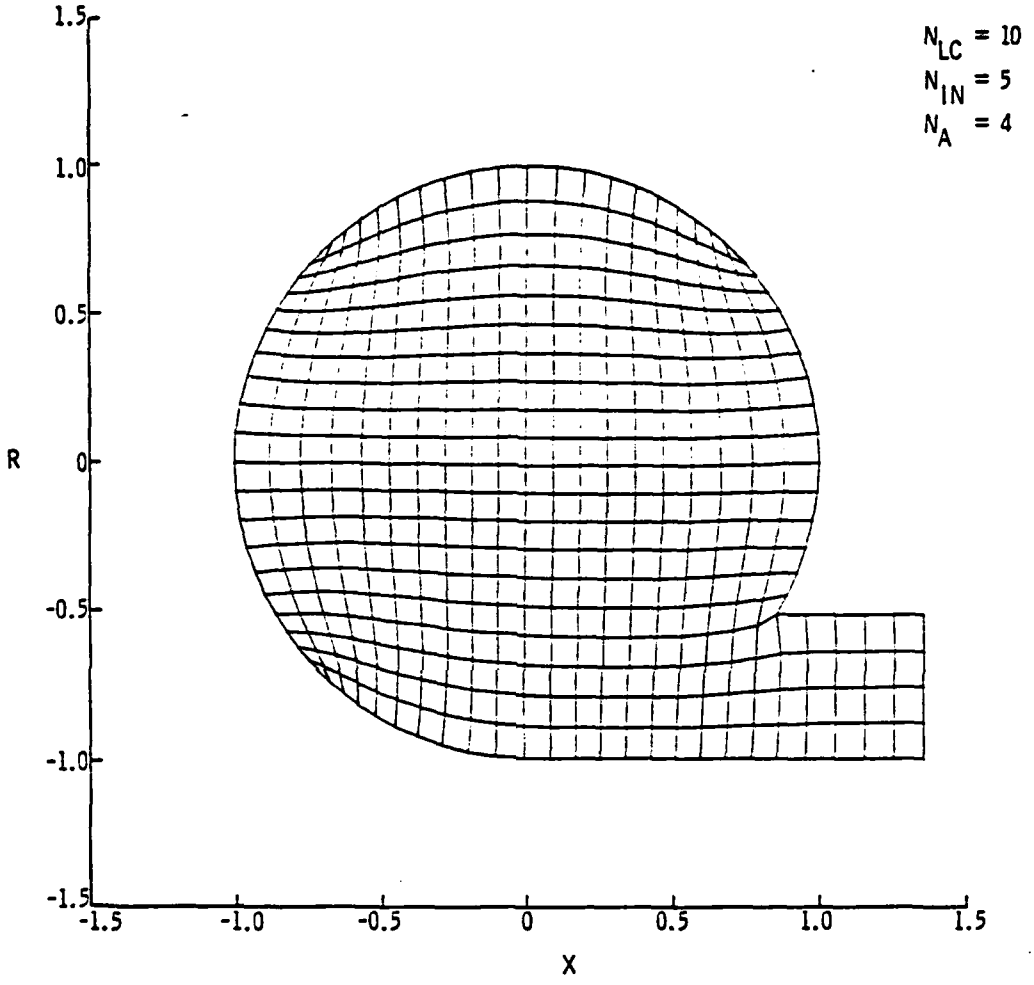

Fig. 5. Collector Grid, Case 1.

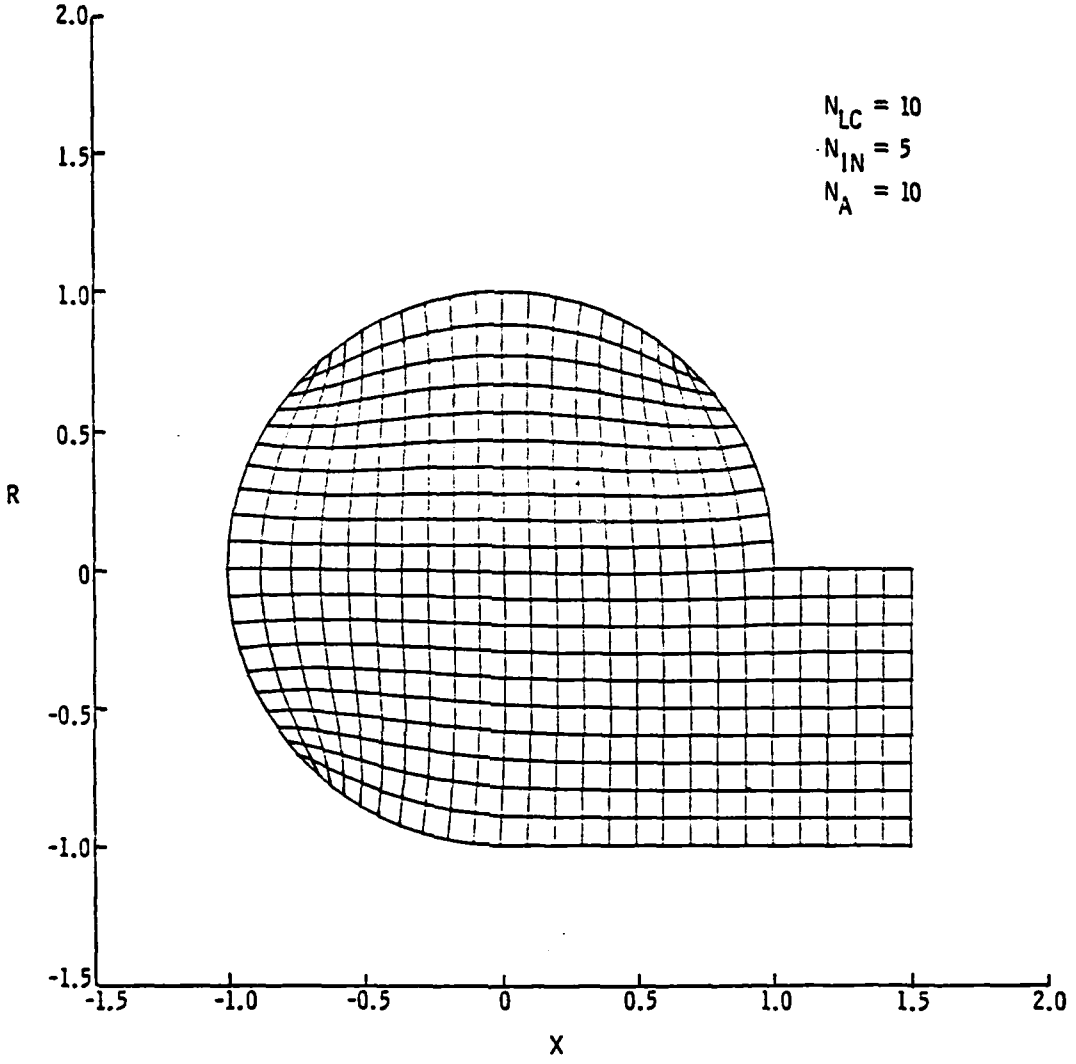

Fig. 6. Collector Grid, Case 2.

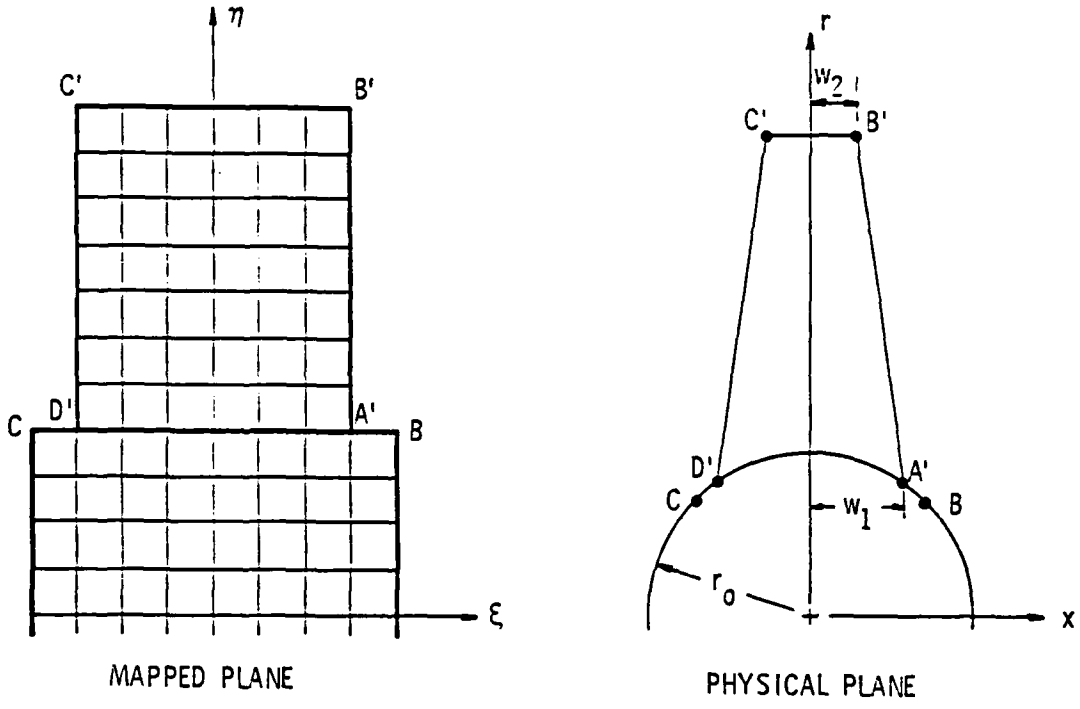

Fig. 7. Exit Pipe Profile Geometry and Grid.

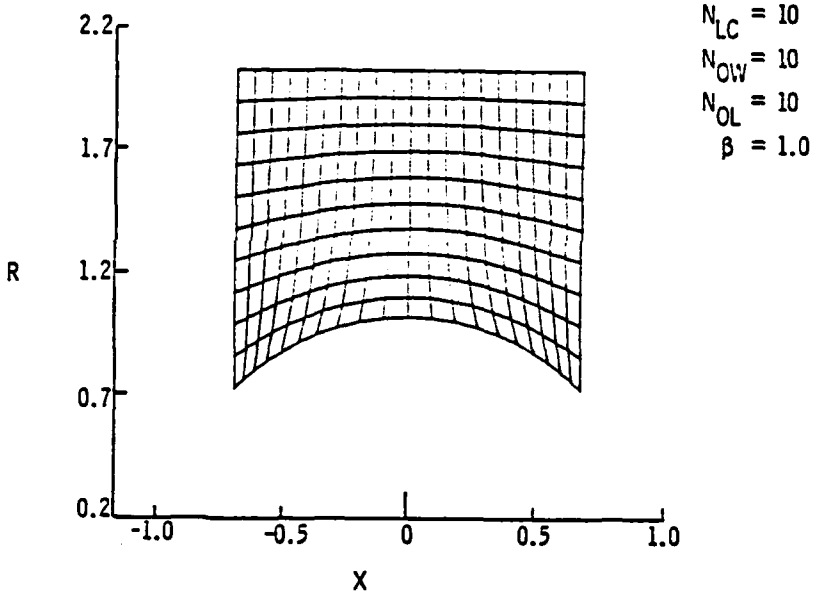

Fig. 8. Exit Pipe Grid, Case 1.

4 October 1984
GHH:lhz

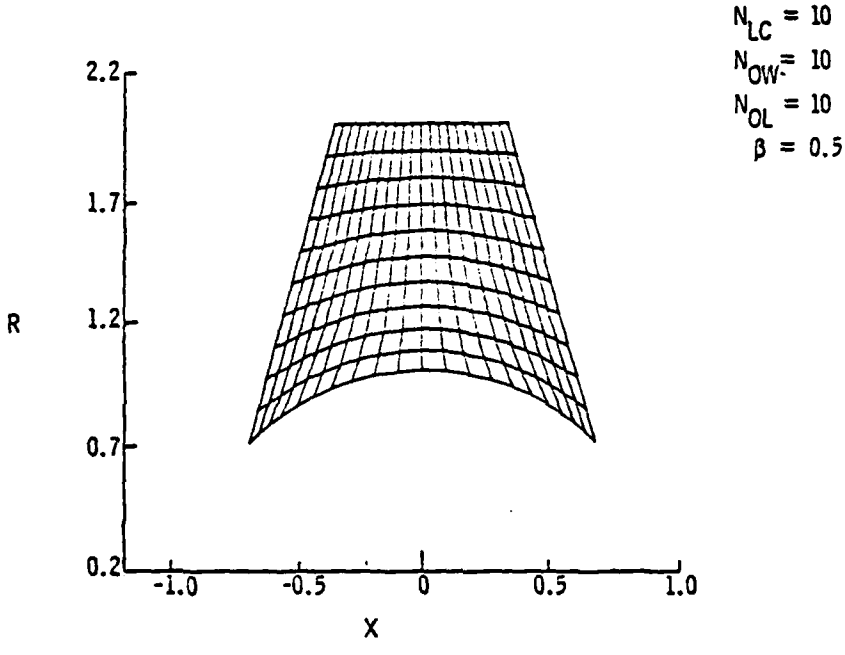

Fig. 9. Exit Pipe Grid, Case 2.

DISTRIBUTION LIST FOR UNCLASSIFIED TECHNICAL MEMORANDUM 85-12,
by G. H. Hoffman, dated 4 October 1984

Office of Naval Research
800 North Quincy Street
Department of the Navy
Arlington, VA 22217
Attn: R. E. Whitehead
(Copy No. 1)

Office of Naval Research
800 North Quincy Street
Department of the Navy
Arlington, VA 22217
Attn: C. Lee
(Copy No. 2)

Commander
Naval Sea Systems Command
Department of the Navy
Washington, DC 20362
Attn: T. E. Peirce
Code NSEA-63R31
(Copy No. 3)

Commander
Naval Underwater Systems Ctr.
Department of the Navy
Newport, RI 02840
Attn: D. J. Goodrich
Code 3634
(Copy No. 4)

Commander
David W. Taylor Naval Ship
Research & Development Ctr.
Department of the Navy
Bethesda, MD 20084
Attn: T. T. Huang
Code 1552
(Copy No. 5)

Commander
David W. Taylor Naval Ship
Research & Development Ctr.
Department of the Navy
Bethesda, MD 20084
Attn: Library
(Copy No. 6)

Commander
Naval Surface Weapons Ctr.
Department of the Navy
Silver Spring, MD 20910
Attn: Library
(Copy No. 7)

Defense Technical
Information Ctr.
5010 Duke Street
Cameron Station
Alexandria, VA 22314
(Copies 8 through 13)

Naval Research Laboratory
Department of the Navy
Washington, DC 20390
Attn: Library
(Copy No. 14)

Superintendent
Code 1424
Naval Post Graduate School
Monterey, CA 93949
(Copy No. 15)

Director
Applied Research Laboratory
The Pennsylvania State University
Post Office Box 30
State College, PA 16804
Attn: S. A. Abdallah
(Copy No. 16)

Director
Applied Research Laboratory
The Pennsylvania State University
Post Office Box 30
State College, PA 16804
Attn: M. C. Brophy
(Copy No. 17)

DISTRIBUTION LIST FOR UNCLASSIFIED TECHNICAL MEMORANDUM 85-12,
by G. H. Hoffman, dated 4 October 1984 [continuation]

Director
Applied Research Laboratory
The Pennsylvania State University
Post Office Box 30
State College, PA 16804
Attn: J. J. Eisenhuth
(Copy No. 18)

Director
Applied Research Laboratory
The Pennsylvania State University
Post Office Box 30
State College, PA 16804
Attn: W. S. Gearhart
(Copy No. 19)

Director
Applied Research Laboratory
The Pennsylvania State University
Post Office Box 30
State College, PA 16804
Attn: W. R. Hall
(Copy No. 20)

Director
Applied Research Laboratory
The Pennsylvania State University
Post Office Box 30
State College, PA 16804
Attn: R. E. Henderson
(Copy No. 21)

Director
Applied Research Laboratory
The Pennsylvania State University
Post Office Box 30
State College, PA 16804
Attn: G. H. Hoffman
(Copy No. 22)

Director
Applied Research Laboratory
The Pennsylvania State University
Post Office Box 30
State College, PA 16804
Attn: K. C. Kaufman
(Copy No. 23)

Director
Applied Research Laboratory
The Pennsylvania State University
Post Office Box 30
State College, PA 16804
Attn: G. C. Lauchle
(Copy No. 24)

Director
Applied Research Laboratory
The Pennsylvania State University
Post Office Box 30
State College, PA 16804
Attn: M. W. McBride
(Copy No. 25)

Director
Applied Research Laboratory
The Pennsylvania State University
Post Office Box 30
State College, PA 16804
Attn: T. E. McDevitt
(Copy No. 26)

Director
Applied Research Laboratory
The Pennsylvania State University
Post Office Box 30
State College, PA 16804
Attn: B. R. Parkin
(Copy No. 27)

Director
Applied Research Laboratory
The Pennsylvania State University
Post Office Box 30
State College, PA 16804
Attn: GTWT Files
(Copy No. 28)

Director
Applied Research Laboratory
The Pennsylvania State University
Post Office Box 30
State College, PA 16804
Attn: ARL/PSU Library
(Copy No. 29)

END

FILMED

3-85

DTIC